Rotor Performance Enhancement Using Slats on the Inner Part of a 10MW Rotor

Gaunaa, Mac; Zahle, Frederik; Sørensen, Niels N.; Bak, Christian; Réthoré, Pierre-Elouan

Published in:
Proceedings og EWEA 2013

Publication date:
2013

Document Version
Publisher's PDF, also known as Version of record

Rotor Performance Enhancement Using Slats on the Inner Part of a 10MW Rotor

Mac Gaunaa, Frederik Zahle, Niels N. Sørensen, Christian Bak, Pierre-Elouan Réthoré
Wind Energy Department, DTU, DK-4000 Roskilde, Denmark
macg@dtu.dk

Abstract

The present work continues the investigations of using slats on the inner parts of wind turbine rotors by using an updated version of the 2D CFD based airfoil/slat design tool earlier used by the authors in combination with the rotor design methods from [8] to design slats for $0.1 > r/R > 0.3$ for the LightRotor baseline 10 MW reference rotor [10]. For the slatted case, a retwisting of the slatted inner part of the rotor was allowed for the slats to be able to work as intended. The new addition to the 2D CFD based design tool is that the representation of the airfoil and slats are done using splines, thus allowing for a much broader design space than in the previous works where only the position, size and additional camber of the slat airfoil could be adjusted. The aerodynamic performance of a slatted rotor is for the first time evaluated using 3D CFD in this work, and the results are compared to predictions of a lifting line based computational tool based on 2D airfoil polars to highlight the 3D rotational effects on airfoil coefficients of the slatted inner airfoil sections.

DISCLAIMER: ERRONEOUS 3D GEOMETRY IN THIS VERSION OF THE PAPER!

The authors have discovered an inconsistency in our definition of the reference frames used to define the chordwise directions in the 2D and 3D cases. This have resulted in the slat not being positioned correctly in the 3D computations, and, additionally, that the retwisting of the main rotor in the slatted case have been done using wrong retwisting values. Therefore, the 3D geometry shown in this version of the work is in fact not as intended. This has an impact on the results, and on the conclusions that can be drawn from them. The error is found, and new computations are being set up in time for the results and analysis thereof to be ready for the next revision round. It is noted in the text/figures whenever the reader should be aware of erroneous results which will change for the next revision of the paper.

1 Introduction

The loading on the inner part of the blades on the majority of MW-size wind turbines is significantly lower than what is required for maximum energy capture. The reason for this is a combination of structural strength/material cost issues, considerations of stand still loads and maximum chordlength constraints due to transportation requirements. In addition, the rotational effects neglected [2] in the standard Blade Element Momentum (BEM) theory used in rotor design cause a lower loading on the inner part of the rotor than what is needed to get an optimal power production. The available maximum power production for designs with ideally loaded inner sections was quantified by Johansen *et.al.* [3], where CFD/Lifting line free wake/actuator disc computations on a rotor designed for maximum power production is shown. Compared to the IEA/NREL/Upwind 5MW Reference Wind Turbine (RWT5) the one-point power production optimized rotor showed an 8% increase in C_P obtainable at the cost of a 12% increase in C_T. This higher loading at the inner sections was accomplished in [3] by increasing the chordlength of the rotor far beyond what would be practical or economically sensible for real turbines.

Recent investigations [4–9], however, have indicated that the use of multiple element airfoils on the inner part of the rotor, where the main airfoil sections have a high relative thickness due to the structural constraints, can increase the lift coefficient, and hence loading, enough to obtain a significant increase in power production without increasing the chordlength of the blade. Gaunaa *et.al.* [4, 5]

presented the use of a leading edge slat airfoil as a likely candidate for increasing the performance of the very thick inboard sections on wind turbine rotors. These studies employed a viscid-inviscid interaction tool to design the slat airfoils. Zahle *et.al.* [6, 7] further extended the investigations by showing the feasibility of using a CFD based optimization tool for the 2D design of slatted airfoils and on the other hand by comparing data from wind tunnel measurements with CFD predictions for a slat/40% thick main airfoil combination. The most recent work by Gaunaa *et.al.* [8] presented aerodynamic design methods for slatted rotors, and quantified the beneficial power producing effect of using slats on the inner part of iteration 1 of the 10MW reference rotor [10] using free wake lifting line methods [11–13] and BEM based methods based on 2D airfoil data. The conclusion was that the power production potential by fitting slats on the inner part of design iteration one of the quite heavily loaded iteration one of the 10MW reference turbine is likely to be more than 1% annual energy production (AEP), but that further work/investigations on the complex rotational effects/stall-delay effects when using slats is needed to assess the increase in AEP more precisely. The work further suggested that the beneficial effects of using slats may be larger if the slats and the main rotor blade are designed simultaneously as opposed to using slats as an add-on to existing unslatted rotor designs.

The present work continues the investigations of using slats on the inner parts of wind turbine rotors by using an updated version of the 2D CFD based airfoil/slat design tool described by Zahle *et.al.* [14] in combination with the rotor design methods from [8] to design slats for $0.1 > r/R > 0.3$ for the LightRotor baseline 10 MW reference rotor [10]. For the design, a retwisting of the slatted inner part of the rotor was allowed for the slats to be able to work as intended. The addition to the 2D CFD based design tool is that the representation of the airfoil and slats are done using splines, thus allowing for a much broader design space than in the previous works where only the position, size and additional camber of the slat airfoil could be adjusted. The aerodynamic performance of a slatted rotor is for the first time evaluated using 3D CFD [15–17], and the results are compared to predictions of a lifting line based computational tool based on 2D airfoil polars to highlight the 3D rotational effects on airfoil coefficients of the slatted inner airfoil sections.

The methods used in the present work is presented in the next section, after which the baseline 10 MW rotor and its standard operational settings are shown. After the results and discussion section, the conclusions are drawn.

2 Methods

The methods used in the present work are outlined in this section. The slat design procedure can be split up into a rotor design part and a 2D slat design part, which builds on the 2D version of the CFD solver EllipSys. The analysis of the aerodynamic performance of the reference rotor and the retwisted, slatted version of the rotor is done with the 3D version CFD code EllipSys using an overset grid method. All methods are described below.

2.1 Rotor Design

A splitting of the rotor design and the airfoil design into two separate parts is possible through the use of either a lifting line or a BEM method approach. In these methods, the 2D airfoil behavior and rotor aerodynamic behavior is decoupled, allowing to link the desired characteristics of the rotor flow to a corresponding 2D airfoil behavior of each radial station. Whether using this approach is valid on the inner part of the rotor will be illuminated later in this work by comparing the expected aerodynamic behavior from the simpler design method, based on 2D airfoil behavior, with the prediction from the 3D CFD method, which does not rely on a splitting of the problem into stripwise 2D solutions, thus enabling true inherently 3D flows to be predicted realistically.

For the free wake lifting line results shown in the present work, the code by Gaunaa was used. The method is based on a free wake lifting line method, where steady state operation is used to speed up the convergence of the solution by use of a non-parabolic solution technique and use of symmetry in the wake. Forces due to drag are added in the relative flow direction using the inviscid force magnitude combined with the lift to drag ratios. The method can be run with either a given circulation distribution or the circulation distribution can be obtained iteratively from the rotor geometry combined with 2D aerodynamic force

coefficients and the lifting line method. Please refer to [11–13] for the details of the method.

The rotor design computations are performed with the lifting line free wake method in the mode where a prescribed circulation distribution is run. From earlier works [13] an analytic expression for the circulation distribution very close to optimal loading is known: using this circulation distribution on the inner part of the rotor and on the outer part of the rotor a circulation distribution corresponding to a lifting line simulation run earlier using 2D airfoil coefficients corresponding to the baseline rotor, we have the target design point solution including the magnitude and direction of the relative wind velocities along the blade as well as the loading from the lifting part of the aerodynamic forces. From these results the target design lift coefficients, based on the original blade chordlengths can be computed. Once the airfoil polars, including the design angles of attack, are known for the 2D optimized slatted sections, the magnitude and direction of the relative wind velocities from the lifting line free wake results are combined with target loading and the 2D design lift coefficient and angle of attack to specify the retwisting of the main rotor and the location of the slat crossection in space.

2.2 Optimization framework

The optimization framework developed for this work is programmed in Python using the open-source Multidisciplinary Design Analysis and Optimization framework OpenMDAO [1] for connecting the different components in the optimization. The optimization assembly consisted of four main components as shown in Figure 1. The objective function was composed of two functions: A_1, which evaluates the lift-to-drag ratio at the target angle of attack; and A_2, which seeks to maximize the lift coefficient at some angle of attack, which the optimizer is free to tune. The two functions A_1 and A_2 are normalized with a predefined reference lift-to-drag ratio and lift coefficient.

$$CostFunc = -(A_1 + A_2) \quad (1)$$

The two functions A_1 and A_2 is defined as

$$A_1 = \frac{C_l(\alpha_{target})}{C_d(\alpha_{target})} \cdot \frac{1}{(C_l/C_d)_{target,ref}} \cdot K_{optim} \quad (2)$$

$$A_2 = \frac{C_l(\alpha)}{C_{l,maxref}} \cdot (1 - K_{optim}) \quad (3)$$

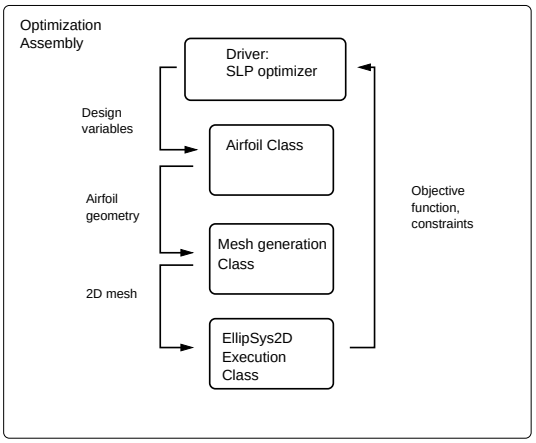

Figure 1: *Schematic of the optimization assembly.*

K_{optim} is a factor in the range [0:1] which biases the cost function towards obtaining the target lift coefficient or lift-to-drag ratio.

The calculation of the objective function was parallelized across 20 cores, with two CFD simulations evaluating C_{l-max} and L/D executed concurrently on 10 cores each. The total time for an optimization was approximately nine hours with ≈340 objective function evaluations.

The shape of the slat airfoil was described using two Bezier splines, one for the pressure side and another for the suction side. Each optimization was initialized with a shape fitted to a FFA-W3-360 airfoil.

The optimization of each airfoil consisted of 17 design variables: the AOA, the trailing edge position and angle of the slat and 13 control points of the Bezier splines.

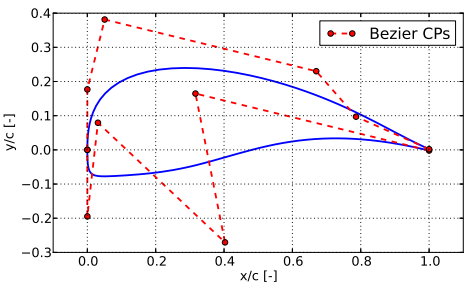

Figure 2: *Normalized slat airfoil showing the control points of the Bezier spline used to describe the slat airfoil shape.*

2.3 CFD solver: EllipSys

The 2D and 3D airfoil aerodynamics used in the present work, including those in the optimization algorithm, are obtained using 2D and 3D versions of DTU's in-house incompressible CFD solver EllipSys. The EllipSys code is a multiblock finite volume discretization of the incompressible Reynolds-averaged Navier-Stokes (RANS) equations in general curvilinear co-ordinates. In the present work the turbulence in the boundary layer is modeled by the $k-\omega$ SST model. The mesh generation is done with HypGrid [19] an in-house hyperbolic mesh generation code. A general description of the EllipSys code is given in [15–17]. A general validation for the capability with multiple element airfoils can be found in [18], and applications to the case of multiple element cases with a thick main airfoil can be found in [4–7], and applications of EllipSys to 3D rotor flows can be found in [3, 11–13].

2.4 Overset grid method

The 3D rotor simulations including the slats were carried out using the overset grid method in EllipSys3D, using the steady state moving mesh method with fully turbulent surface flow modeled by the $k-\omega$ SST model. The automated holecutting method implemented in the solver makes it possible to generate grids with geometries in very close proximity. This method attempts to create a grid with the best mesh compatibility in the overlap regions, while minimizing the number of fringe cells that do not have valid donors. The rotor mesh consisted of a total of 1236 blocks of 32^3 with 1092 blocks in the rotor mesh and 48 blocks in each of the slat meshes totalling approximately 40×10^6 cells. The mesh consisted of a total of 334000 fringe cells with 156 orphan points. Figure 3 shows a slice of the mesh at a radius of $r/R=0.17$.

3 Main rotor

The LightRotor 10 MW reference rotor is described by Bak *et.al.* in [10], and has radius $R=89.16m$. The blade is designed using the FFA-W3-xxx series airfoils since these airfoils are publically available and have a weight on the higher relative thicknesses required for limiting the weight of the rotor. Please refer

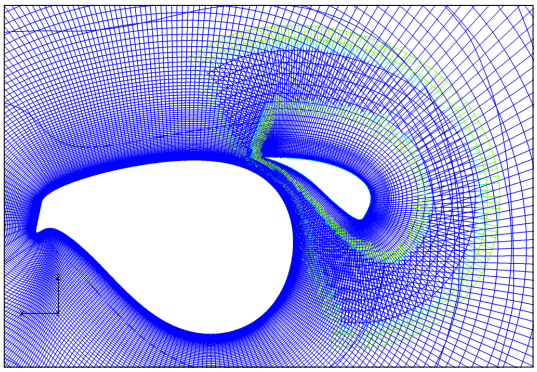

Figure 3: *A slice of the computational overset grid at a radius of* $r/R=0.17$.

to the original reference for details on the design and design choices [10]. In order to asses the potential of using slats on the rotor, it was chosen to allow a retwisting of the inner part of the main blade in the slatted case. This is because the angle of attack for which the combined main airfoil/slat combination is effective lie quite far from the one for the main airfoil alone, making it harder to design a well-functioning slat as a retrofit to a main wing of fixed geometry than if the main wing is allowed to be retwisted.

4 Results and Discussion

4.1 Rotor Design

The rotor design computations were performed as described earlier. Figure 4 show the key result from these computations: the required target lift coefficient for the slatted rotors and the flow angle of the resulting flow along the blade.

It is seen that in order to obtain the optimal power production from the lift forces, the lift coefficient needs to be quite large with the given size of the chordlenght on the main rotor. Values in this range, however, is plausible with slats of approx 30% of the main chordlenght.

4.2 Slat Design

4.2.1 2D Crossection Design

2D optimizations were carried out for slats corresponding to five locations along the blade: r/R=0.10, 0.15, 0.20, 0.25 and 0.30 with relative thicknesses of the main airfoil of 0.91, 0.72, 0.58, 0.45 and 0.36, respectively. Target lift coefficient operation points was obtained from

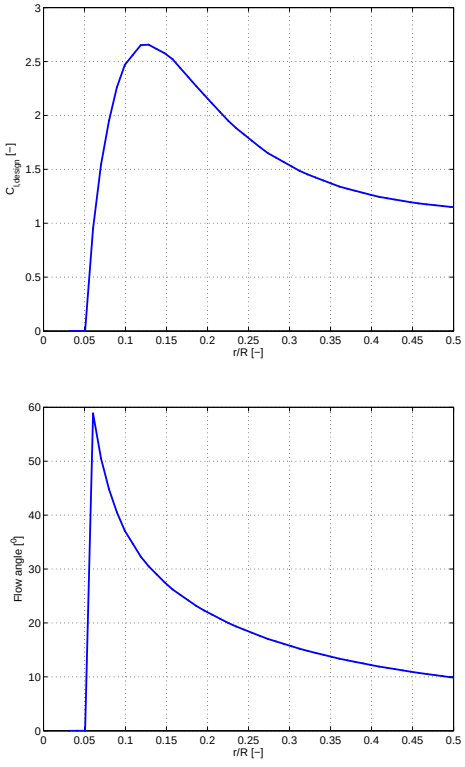

Figure 4: *Design/target lift coefficient (upper) and flow angle (lower).*

the free-wake lifting line method. Except for the innermost section, all sections reached the target lift coefficients at approx. 5 deg below C_{l-max}. Figure 5 and Figure 6 show the 2D lift and drag coefficients for the slatted airfoil sections. It is noted, that the total lift coefficients of the slatted versions of the very thick sections obtain very high values. The geometric layout of the crossections are shown in Figure 9.

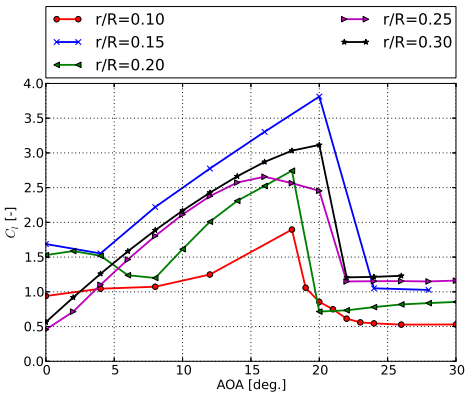

Figure 5: *Lift coeffient vs angle of attack for the five multi-element airfoils.*

As a typical example of the details of the 2D flow, Figure 7 and Figure 8 show the pressure

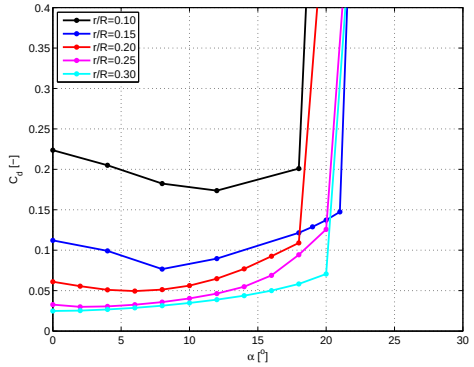

Figure 6: *Drag coeffient vs angle of attack for the five multi-element airfoils.*

coefficient and contours of the velocity magnitude of the flow around the airfoil, respectively. The airfoil shape correspond to the radial station $r/R = 0.15$, for which the main airfoil has a relative thickness of $t/c = 0.72$.

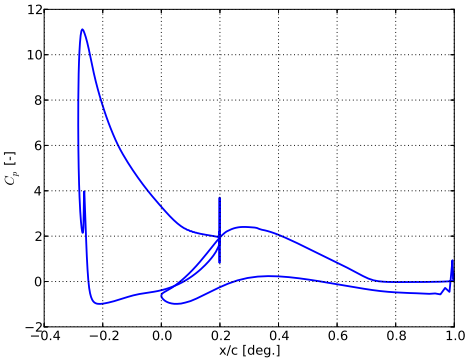

Figure 7: *Pressure distribution at AOA = 20 deg for the r/R = 0.15 section.*

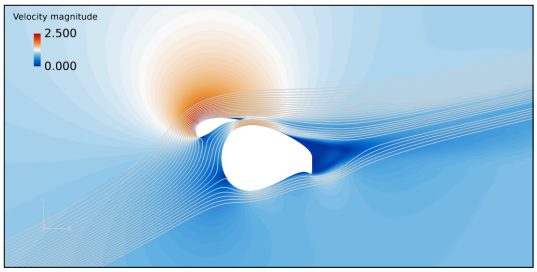

Figure 8: *Contours of velocity magnitude of the flow around the airfoil at AOA = 20 deg for the r/R = 0.15 section.*

It is noted that the majority of the forces stems from the slat airfoil.

4.2.2 3D Layout

The 3D shape of the slat is shown in Figure 9 along with the crossectional shapes. Furthermore, a view of the slatted rotor from a downwind position is shown in Figure 10 to give an impression of the size of the slats relative to the main rotor.

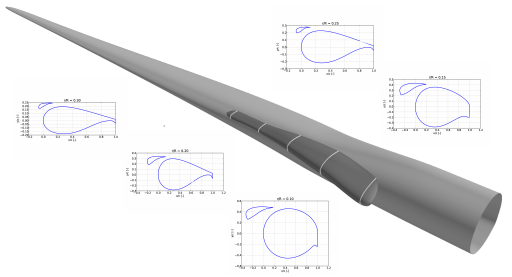

Figure 9: *The Light Rotor 10 MW reference blade fitted with a leading edge slat extending from 8% span to 32% span. The design radii* r/R *=[0.10 0.15 0.20 0.25 0.30] are outlined.*

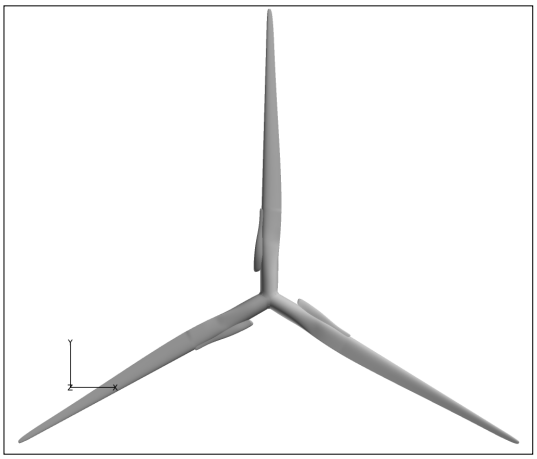

Figure 10: *A rear view of the rotor with slats.*

4.3 Performance Evaluation

DISCLAIMER: NOTE THAT FOR ALL 3D RESULTS IN THE REMAINDER OF THIS WORK, THE 3D GEOMETRY IS NOT AS INTENDED. THIS WILL BE CORRECTED IN THE NEXT VERSION OF THE PAPER.

In order to evaluate the performance of the slatted rotor, Figure 11 compare the surface streamlines in the slatted and the unslatted cases at the design point.

It is seen that the flow is significantly affected by the slat. Even though there is some radial component of the flow present on the slat, it

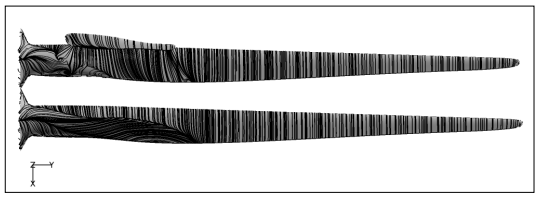

Figure 11: *Surface streamlines on the 10MW reference blade (upper) and for the 10MW blade fitted with slats on the inner part (lower).*

is evident that the slat airfoils are not stalling. Apart from this it is noted that the effect of the tip of the slat can be seen clearly on the streamline pattern on the main blade.

In order to further assess the effect of the slat in a qualitative manner, Figure 12 show a visualization of the vorticity at radial positions $r/R = 0.15$ (upper) and $r/R = 0.25$ (lower), with (left) and without (right) slats.

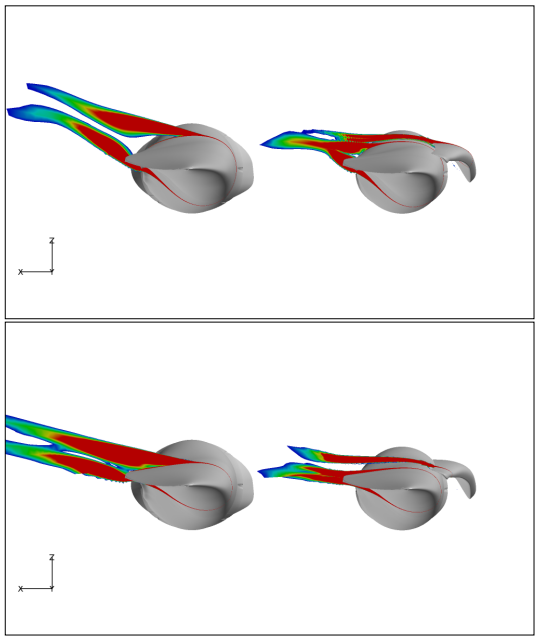

Figure 12: *Visualization of the effect of adding slats to the 10MW reference rotor. Vorticity magnitude. Upper:* $r/R = 0.15$*, lower:* $r/R = 0.25$*, left: baseline rotor, right: slatted rotor.*

The relative thicknesses of the main airfoil at these sections is $t/c = 0.72$ and $t/c = 0.45$, respectively. It is seen that the flow is attached on the slat airfoil, and that the stalling is suppressed significantly on the main rotor. Additionally, it is observed that the angle that the flow leaves the rotor is changed when the slat is added. This is because the effect of the increased thrust force results in a lower axial ve-

locity in the slatted case.

In order to show a more quantitative result, Figure 13 show the local thrust and power coefficients for the baseline and the slatted rotor.

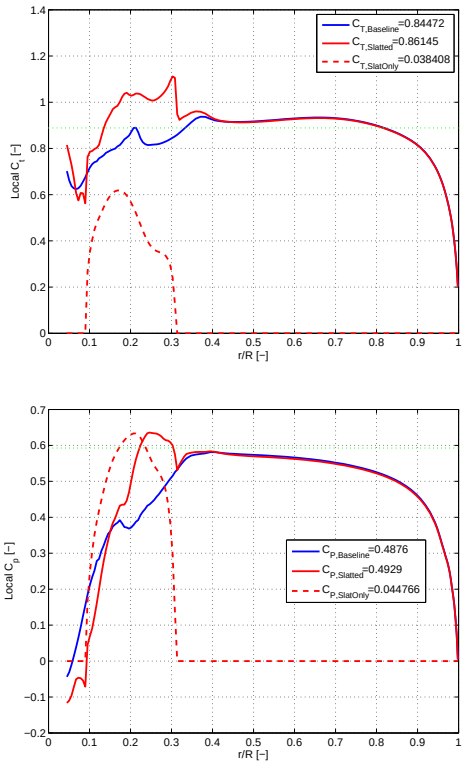

Figure 13: *Local thrust coefficient (upper) and local power coefficient (lower) for the baseline rotor (blue) and slatted rotor (red) as function of nondimensional radial position. The dashed curve signify the contribution of the slat part isolated.*

It is seen that the local thrust and power coefficient increase significantly on the inner part of the rotor. It is also observed that the slat itself accounts for a very big part of the forces. This is seen to be very much the case for the local power coefficient. This is in agreement with the behavior of slatted airfoils in 2D, where it is seen that the force component in the direction of the free stream flow from the slat is often negative. Usually this is more than outweighed by an added force component in that direction from the main airfoil. It is seen that the local thrust coefficient is significantly higher than 8/9, which may be partly due to the error in the geometry of the 3D case. Another interesting feature can be seen in the results: the local thrust and especially the local power coefficient is somewhat lower in the slatted case than in the unslatted case for outer part of the blade where slats are not mounted. In a BEM based computational tool this would not be the case due to the assumption of streamtube independence. In order to further illuminate this feature, Figure 14 show the shape of the cumulative difference in integral C_T and C_P when integrating from the root toward the tip.

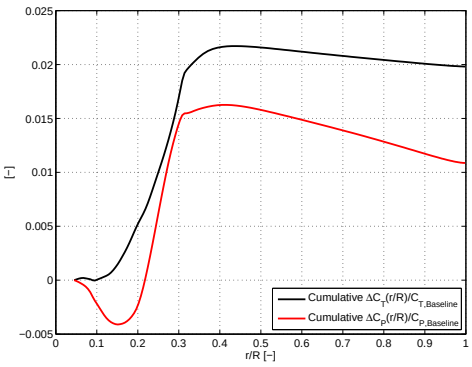

Figure 14: *Normalised cumulative thrust and power increase due to the addition of slats.*

The effect is seen more clearly here because the local coefficients are multiplied with $2r/R$ when integrating up for the integral rotor values C_T and C_P (see [8]). It is seen that 50% of the power production increase is lost again on the outer part of the blade, from 40% radius to the tip. It is also evident that the slatted rotor performs worse than the baseline case inside of 15% radius.

5 To-Do list when the simulation data from the correct 3D geometry is available

- Redo all figures based on 3D results
- Compute also cases corresponding to rotor at rated RPM before power limit
- From the results from the point above, quantify the increase in AEP based on the 3D CFD results (as in [8], but based on CFD results)
- Compare with results from a BEM approach using 2D input airfoil data to assess the 3D rotational effects on airfoil coefficients of the slatted inner airfoil sections

6 Conclusion

The present work aims at investigating the power production potential of adding slats to the inner part of a typical MW size wind turbine by fitting the 10MW LightRotor reference turbine with slats on the inner part $0.1 > r/R > 0.3$. The design point for the rotor loading is determined using a lifting line free wake method.

A new optimization framework for airfoils using 2D CFD has been demonstrated. A set of multi-element airfoils were designed for the Light Rotor 10 MW reference turbine, which, except for the $r/R = 0.10$ airfoil met the target operation points derived from lifting line simulations.

The present paper show for the first time 3D CFD simulations of a horizontal axis wind turbine fitted with leading edge slats.

Comparing the results from 3D simulations of the slatted rotor to the baseline rotor, it is seen that the slats modify the flowfield on the inner part of the rotor significantly. However, due to the error in the geometry pointed out earlier it has not been possible to precisely quantify precisely the beneficial effect of the slats on the power production. The results from the simulations on the erroneous geometry have shown an increase in C_P of 1% with a corresponding increase in C_T of 2%. It is believed that the correct geometry will perform better than this, but the results in the next version of the paper will show wether this is correct.

The 3D CFD results further showed that the highly loaded slatted region causes the thrust, and to a higher degree, the power to be reduced compared to the baseline rotor on the outer part of the rotor (>40% radius), where there are no slats. This result is in direct contradiction with what would be the result from a BEM based method, where the streamtube independence renders the highly loaded inner slatted sections aerodynamically "invisible" to the outer sections. For the investigate case (with the erroneous 3D geometry) the power lost on the outer part of the rotor corresponds to 50% of the increase in power due to the addition of the slats.

Acknowledgements

It is gratefully acknowledged that this work was funded by the Danish Energy Agency within the EUDP2010-I Light Rotor project.

References

[1] OpenMDAO website *http://openmdao.org.*

[2] Madsen, H.Aa. *Two modifications of the BEM method based on validation with results of actuator disc results* In Research in Aeroelasticity EFP-2006. RisøReport 1611. 2006

[3] Johansen, J., Madsen, H, Aa., Gaunaa, M. and Bak C. *Design of a wind turbine rotor for maximum aerodynamic efficiency* Wind Energy, Vol. 12, 2009, p 261-273.

[4] Gaunaa, M., Sørensen, N. N. and Bak, C. *Thick Airfoils & High Lift* Chapter in: Research in Aeroelasticity, EFP-2007-II. Ed. Thomas Buhl. Risø-R-1698(EN). 2009.

[5] Gaunaa, M. & Sørensen, N. N. *Thick multiple element airfoils for use on the inner part of wind turbine rotors* In The Science of Making Torque from Wind, Crete, Greece, June 2010.

[6] Frederik Zahle, Mac Gaunaa, Niels N. Sørensen & Christian Bak *Design of a Thick, Flatback, Multi-Element High-Lift Airfoil*. Chapter in Aeroelastic Optimization of MW Wind Turbines, Risø-DTU, Technical Report, Risø-R-1803(EN), December 2011.

[7] Frederik Zahle, Mac Gaunaa, Niels N. Sørensen & Christian Bak *Design and Wind Tunnel Testing of a Thick, Multi-Element High-Lift Airfoil*. EWEA conference Copenhagen 2012. Scientific conference paper.

[8] Gaunaa, M., Zahle, F., Sørensen, N.N., Bak, C. *Quantification of the Effects of Using Slats on the Inner Part of a 10MW Rotor* EWEA conference Copenhagen 2012. Scientific conference paper.

[9] Ragheb A.M., Selig, M.S.. *Multi-Element Airfoil Configurations for Wind Turbines* AIAA 2011-3971, 29th AIAA Applied Aerodynamics Conference, 27 - 30 June 2011, Honolulu, Hawaii.

[10] Christian Bak, Robert Bitsche, Anders Yde, Taeseong Kim, Morten Hansen, Frederik Zahle, Mac Gaunaa, Jakob Wedel Heinen, Tim Behrens. *Light Rotor: The 10MW reference wind turbine* EWEA conference, Copenhagen, Denmark, 2012. Extended abstract submitted.

[11] Gaunaa, M & Johansen, J. *Can CP be Increased by the Use of Winglets? – or – A Theoretical and Numerical Investigation of the Maximum Aerodynamic Efficiency of Wind Turbine Rotors with Winglets*, 46th AIAA Aerospace Sciences Meeting and Exhibit, 7-10 January 2008, Reno, Nevada.

[12] Gaunaa M., Rethore P.-E. & Sørensen N.N. *Internal report: Efp07-ii 33033-0243, Design og optimering af vingetipper for vindmller, risø contribution to final report*. Technical report, DTU, 2011.

[13] Mac Gaunaa, Pierre-Elouan Réthoré, Niels N. Sørensen and Mads Døssing *A computationally efficient algorithm for the aerodynamic response of non-straight blades*. EWEA conference 2011.

[14] Frederik Zahle, Mac Gaunaa, Niels N. Sørensen & Christian Bak. *Multiple-element airfoil optimization for a next-generation Light Rotor* Torque conference, Oldenburg, Germany, 2012. Abstract submitted.

[15] Michelsen J.A. *Basis3D - a Platform for Development of Multiblock PDE Solvers.* Technical Report AFM 92-05, Technical University of Denmark, 1992

[16] Michelsen J.A. *Block structured Multigrid solution of 2D and 3D elliptic PDE's.* Technical Report AFM 94-06, Technical University of Denmark, 1994

[17] Sørensen N.N. *General Purpose Flow Solver Applied to Flow over Hills.* Risø-R-827-(EN), Risø National Laboratory, Roskilde, Denmark, June 1995

[18] Sørensen, N. N. *Prediction of Multi Element Airfoils With the EllipSys Code* Chapter in: Research in Aeroelasticity, EFP-2007-II. Ed. Thomas Buhl. Risø-R-1698(EN). 2009.

[19] Sørensen, N.N., *HypGrid2D, a 2-D mesh generator.* Technical report, Risø-R-1035(EN), Risø National Laboratory, 1998.